

Electronic Supplementary Material (ESI)

**Multicomponent Synthesis via Acceptorless Alcohol
Dehydrogenation: An Easy Access to Tri-Substituted Pyridines**

Hima P., Vageesh M. and Raju Dey*

Department of Chemistry, National Institute of Technology Calicut, Kozhikode, 673601, India

| | | |
|-----------|---|--------------|
| 1 | General information | 2 |
| 2 | Experimental procedure | 2 |
| 3 | Catalyst synthesis | 2-3 |
| 4 | Materials characterization | 4-7 |
| 5 | Qualitative detection of hydrogen | 8 |
| 6 | Heterogeneity test of the catalyst | 8-9 |
| 7 | Recyclability test of the catalyst | 9 |
| 8 | NMR data of compounds | 10-14 |
| 9 | References | 15 |
| 10 | ¹H and ¹³C NMR spectra | 16-29 |

1. General information

All experiments were carried out under an inert argon atmosphere. All the solvents were distilled before use. Unless otherwise noted, all starting materials were purchased from commercial sources and used without any further purification. Analytical thin layer chromatography (TLC) was carried out on Merck 60 F254 pre-coated silica gel plate (0.2 mm thickness). All the products were isolated by chromatography on a silica gel (60-120 mesh) column using hexane and ethyl acetate as eluent.

^1H NMR spectra were recorded on a JEOL 500 MHz NMR spectrometer. As an internal standard, chemical shifts of protons are calibrated using tetramethylsilane (TMS: δ 0.0 ppm). ^{13}C NMR spectra were recorded at a 125 MHz magnetic field and referenced to the carbon resonances of the solvent (CDCl_3 : δ 77.0 ppm). Peaks are labeled as singlet (s), broad singlet (br), doublet (d), triplet (t), double doublet (dd), and multiplet (m). Deuterated chemicals were purchased from Cambridge Isotope Laboratories (CIL). The liberated gas is identified using a GC chromatogram (Shimadzu GC-2010 Plus) by TCD detector.

2. General Procedure for Synthesis of 2,4,6-tri Substituted Pyridines

In an oven-dried high-pressure tube, primary alcohol (0.25 mmol), acetophenone (0.6 mmol), NH_4OAc (1 mmol, 231 mg), catalyst (25 mg), and a tiny magnetic stir bar was added in teflon screw-capped pressure tube. The reaction mixture was purged with argon thoroughly. The reaction mixture was then placed in a preheated heating block at 150 °C. After the completion of the reaction (TLC), the reaction mixture was filtered using celite using ethyl acetate. The filtrate was dried using a rotary evaporator, volatile impurities were removed under vacuum, and further product purification was carried out by silica gel column chromatography using hexane and ethyl acetate as eluent.

3. Catalyst Synthesis

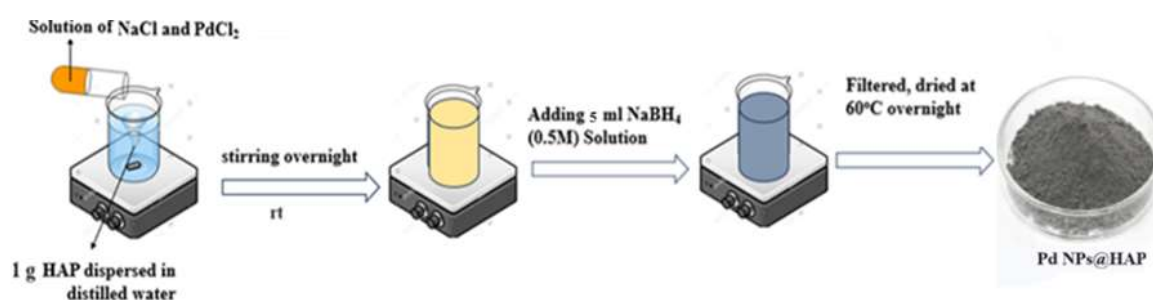
3.1. Synthesis of hydroxyapatite

$(\text{NH}_4)_2\text{HPO}_4$ (40 mmol, 5.28 g) was dissolved in 150 mL of deionized water and the pH was adjusted to 11 with an aqueous ammonia solution. To an aqueous solution of $\text{Ca}(\text{NO}_3)_2 \cdot \text{H}_2\text{O}$ (66.0 mmol, 15.5 g), aqueous ammonia solution was added dropwise to adjust the pH=11. Using a pressure equalizer $(\text{NH}_4)_2\text{HPO}_4$ solution was added dropwise to $\text{Ca}(\text{NO}_3)_2 \cdot \text{H}_2\text{O}$ solution at room temperature over a period of 30 minutes. The solution turned into milky white

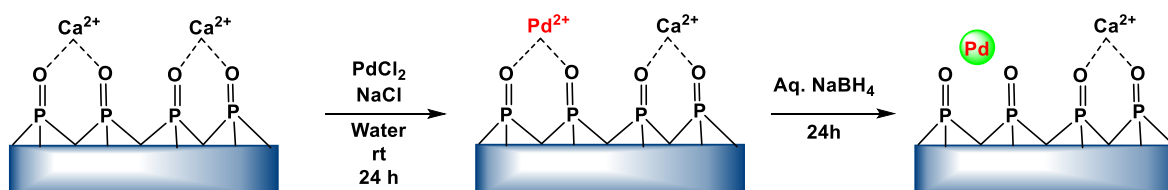
and was heated at 90 °C for another 10 minutes. The precipitate formed was filtered, washed with deionized water and dried at 110 °C

3.2 Synthesis of hydroxyapatite-supported Pd @HAP

1.0 g Hydroxyapatite was dispersed into 100 mL distilled water with constant stirring for 1 h at room temperature. Then 5 mL aqueous solution NaCl (0.2 M) with PdCl₂ (10 mg) was added under stirring for 24 h at room temperature. 5 mL NaBH₄ (0.5 M) was added to reduce Pd (II) to Pd (0) and further stirred for 24 h at room temperature. The grey-black product was filtered and washed three times with deionized water. Finally, the prepared catalyst was dried at 70 °C overnight. The catalyst is labeled as Pd NPs@HAP, and was stored under an argon atmosphere.



Scheme S1. Synthesis of Pd NPs@HAP



Scheme S2. Schematic representation of grafting of palladium on hydroxyapatite surface

4. Material Characterisation

The synthesized palladium loaded on hydroxyapatite was characterized using various technical analyses. The crystallinity and structural composition of the synthesized materials were ensured by X-ray diffraction (XRD) analysis at room temperature using a Malvern Pananalytical diffractometer with Cu K α radiation source ($\lambda = 1.5406 \text{ \AA}$), operated at 45 kV and 40 mA. Fourier transform infrared equipped with FT-IR using a KBr pellet was carried out using a Jasco FT/IR 4600 spectrometer. UV–Visible spectra were recorded between 200 and 800 nm with a Perkin Elmer spectrometer UV/Vis (Lambda 750). The spectra were collected using BaSO₄ as the standard reference. Surface topology and morphology of particles were investigated using a SIGMA 300 scanning electron microscope equipped with energy dispersive spectroscopy (SEM-EDS). The TEM micrographs were obtained on a JEOL JEM-2100 high-resolution scanning/ transmission electron microscope. Surface chemical states were investigated by X-ray photoelectron spectroscopy (XPS) measurement with a Thermo Scientific™ ESCALAB™ Xi+. The specific surface areas were determined from the nitrogen adsorption/desorption isotherms using the BET (Brunauer-Emmett-Teller) method.

4.1. UV-Visible spectra.

Palladium nanoparticle formation has been investigated using UV-visible spectroscopy in the 200-800 nm range. The absence of the absorption peaks above 300 nm in all of the samples shows the full reduction of the initial Pd (II) ions.

4.2. N₂ adsorption-desorption isotherms.

The nitrogen adsorption-desorption isotherm plots were recorded to be classified as type IV and the surface area calculated by the BET method (determined from the desorption branch) was $86.496 \text{ m}^2 \text{ g}^{-1}$

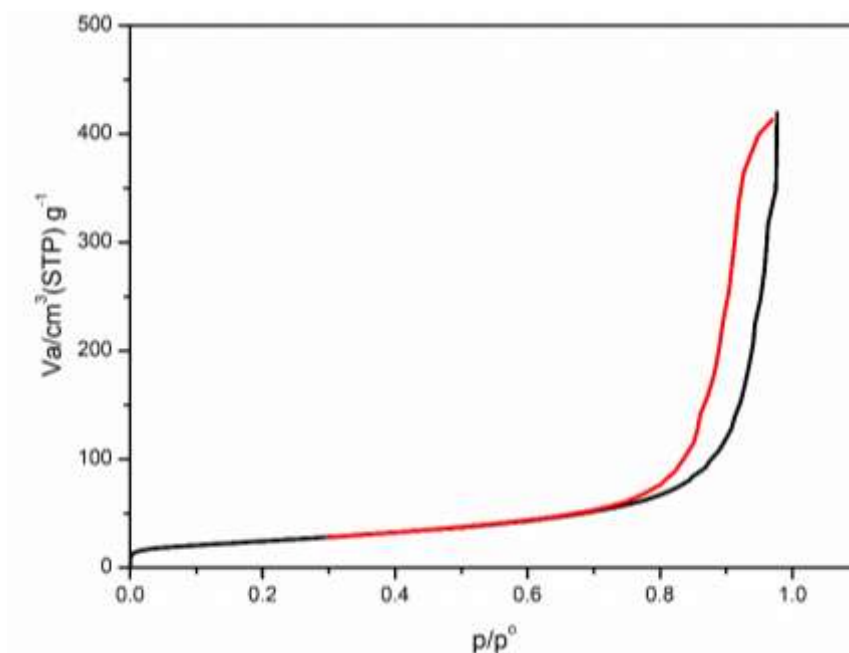


Figure. S1. N₂ adsorption-desorption isotherms for Cu NPs@ HAP catalyst determined using the BET (Brunauer-Emmett-Teller) method.

| | | |
|------------------------------------|--------|--|
| V_m | 19.873 | [cm ³ (STP) g ⁻¹] |
| $a_{s,BET}$ | 86.496 | [m ² g ⁻¹] |
| C | 232.3 | |
| Total pore volume($p/p_0=0.976$) | 0.6488 | [cm ³ g ⁻¹] |
| Mean pore diameter | 30.004 | [nm] |

Table S1. Chemical analysis of copper, SBET area, pore diameter, and grain size of the catalyst by BET

Moreover, the pore size and pore volume were found as 30.004 nm and 0.6488 cm³.g⁻¹ respectively.

4.3. Morphological analysis.

The energy dispersive spectroscopy (EDS) of Pd NPs@HAP was performed along with SEM analysis in different selected zones of Pd NPs@HAP surface confirmed the presence of elemental Ca, Cu, P, O and Pd.

TEM images show the presence of homogeneously distributed palladium nanoparticles on the HAP surface. The sizes of the particles are in the range of 10-20 nm. The high-resolution TEM

image of Pd NPs@HAP shows the high crystallinity of the palladium (0) nanoparticles and the crystalline spacing of 0.2 nm agrees with the [111] lattice spacing of palladium.

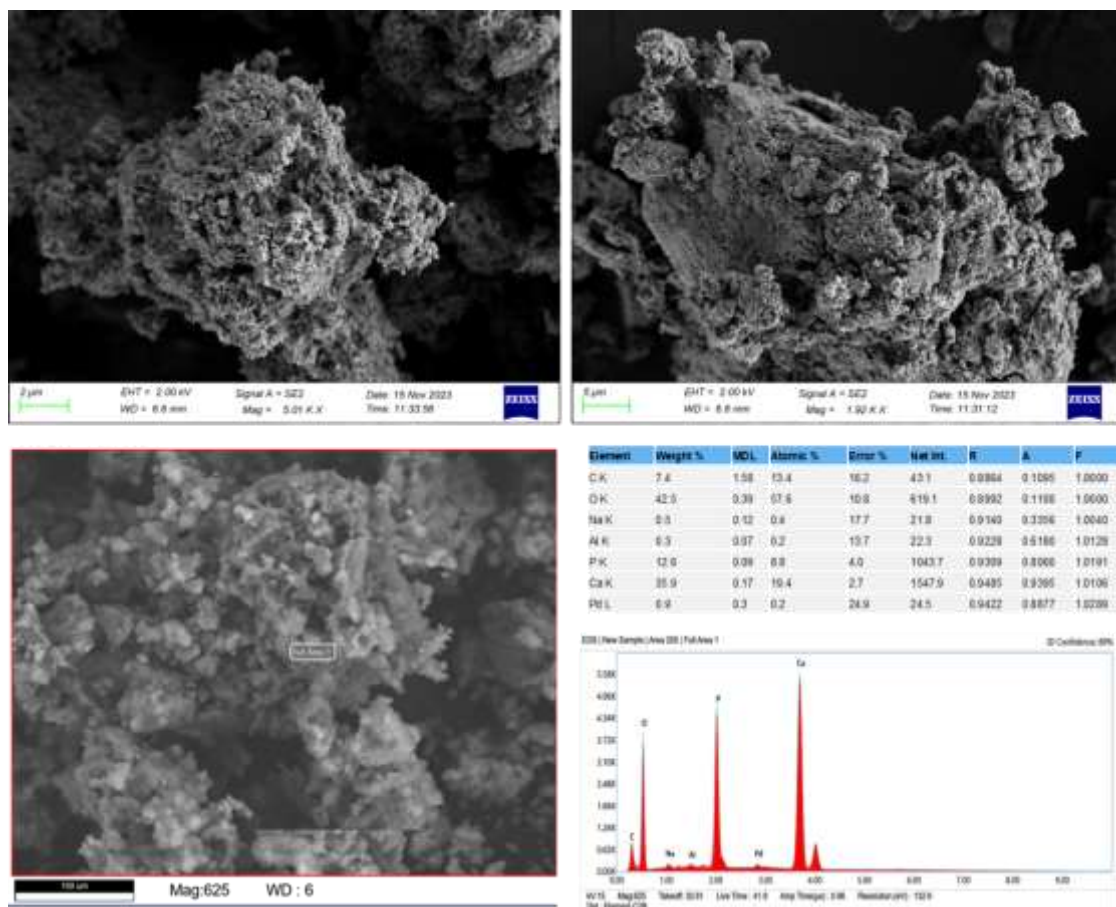


Figure S2. SEM image of palladium on hydroxyapatite.

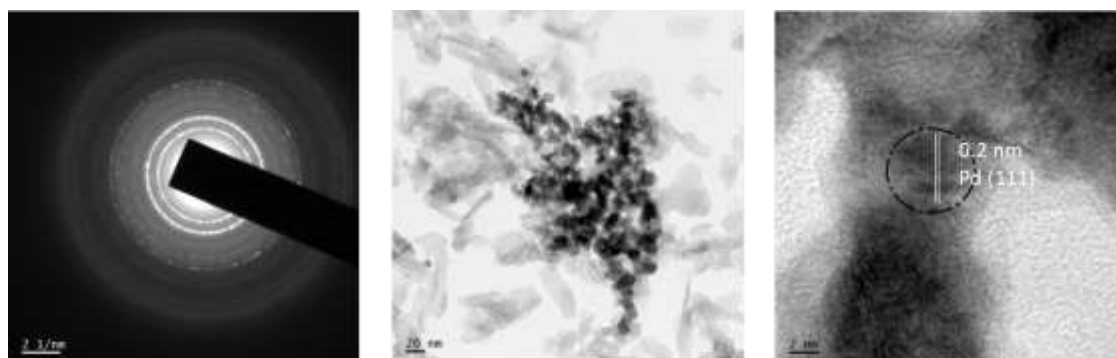


Figure S3. TEM image of Pd NPs@HAP shows the palladium nanoparticle has an average size of 10-20 nm and has a lattice fringe 0.2 nm corresponds to the metallic palladium of (111).

4.4. Structural studies.

The crystallinity and structural composition of the synthesized materials were ensured by X-ray diffraction (XRD) analysis at room temperature. Powder XRD diffraction patterns of Pd NPs@HAP exhibited a broad reflection corresponding to the hydroxyapatite support. Three additional reflections were found in the XRD pattern ($2\theta = 39^\circ$, 46° and 65°) which could be attributed to Pd(0). FTIR spectra of HAP and Pd NPs@HAP shows characteristic tetrahedral PO_4^{3-} peaks are at $472\text{--}600\text{ cm}^{-1}$ and $1032\text{--}1090\text{ cm}^{-1}$. Moreover, the peak at 965 cm^{-1} is for $\text{PO}_4^{3-}(\nu_1)$ and the peaks at 1092 and 1035 cm^{-1} are due to $\text{PO}_4^{3-}(\nu_3)$. The peak at 1395 cm^{-1} is assigned to CO_3^{2-} . The intensity of the carbonate peak is reduced and slightly shifted in the case of Pd NPs@HAP. This may be due to the incorporation of Pd with HAP.

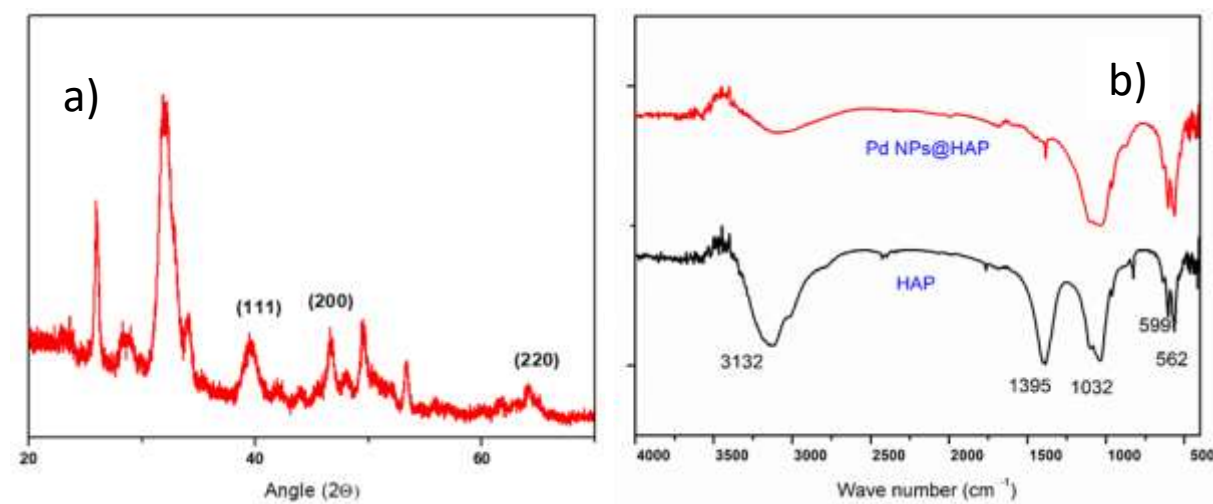


Figure S4. a) XRD spectra of the material analysed at room temperature using a Malvern Panalytical diffractometer with Cu K α radiation source ($\lambda = 1.5406\text{ \AA}$), operated at 45 kV and 40 mA. b) FTIR spectra of the HAP and Pd NPs@HAP spectra recorded at 25°C using KBr pellet

4.5. Elemental analysis

The elemental analysis and chemical states of palladium on the surface of the Pd NPs@HAP catalyst were determined by XPS analysis. The XPS spectra of Ca 2p, P 2p, and O 1s are characteristic of phosphorus, calcium, and oxygen in hydroxyapatite. The 2p peaks at 133.8 eV and 132.9 eV are assigned to the phosphorous in hydroxyapatite. The Ca 2p spectra are composed of two peaks Ca 2p $_{1/2}$ and Ca 2p $_{3/2}$. The binding energy of O 1s consists of two peaks

at 531.62 eV and 530.92 eV associated with the presence of O-P and O-H groups in hydroxyapatite, respectively. The binding energy analysis of Pd revealed two predominant distinct Pd 3d doublets ($3d_{5/2}$ and $3d_{3/2}$) at 335.3 eV, 340.6 eV indicative of Pd (0). Palladium nanoparticle formation has been further investigated using UV-visible spectroscopy in the 200-800 nm range. The absence of absorption peaks above 300 nm in all of the samples shows the full reduction of the initial Pd (II) ions and the formation of Pd (0) nanoparticles.

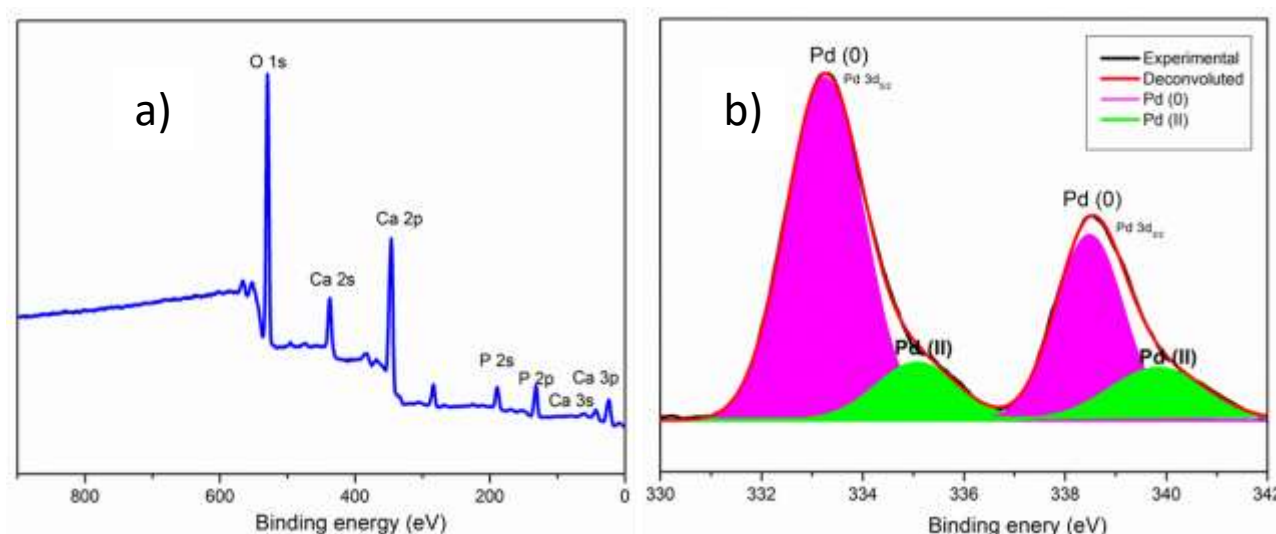


Figure S5. XPS analysis: a) Elemental analysis of Pd NPs@HAP shows the support hydroxyapatite composed of calcium, phosphorous, and oxygen. b) binding energy value for 'Pd' in Pd NPs@HAP

5. Qualitative detection of hydrogen

In an oven-dried high-pressure tube, primary alcohol (0.25 mmol), acetophenone (0.6 mmol), NH_4OAc (1 mmol, 231 mg), catalyst (25 mg), and a tiny magnetic stir bar was added in in a reaction vessel. The reaction mixture purged with argon thoroughly and closed using a septum. The reaction mixture was then placed in a preheated heating block at 150 °C. After 2 hrs, the gas collected using a syringe was subjected to GC analysis and the retention time matched with a sample collected from a hydrogen cylinder of 99.9% purity.

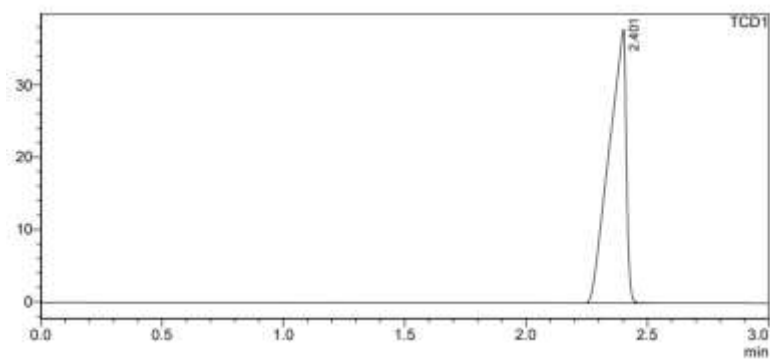


Figure S6. GC Spectrum for evolved gas (TCD mode).

6. Heterogeneity test of the catalyst

To verify the heterogeneous nature of the catalyst, we have used a mercury poisoning test. The standard reaction is carried out in the presence of metallic mercury (200 mg) and compared the reactions. We identified that there was no notable difference in the reaction and we got a similar conversion as that of the reaction without adding mercury. This eliminates the possibility of metal leaching and confirms the heterogeneous nature of the catalyst.

7. Recyclability test of the catalyst.

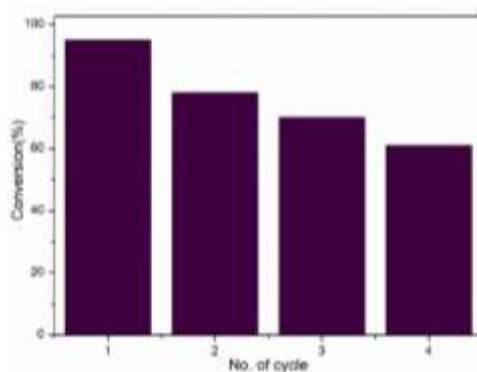
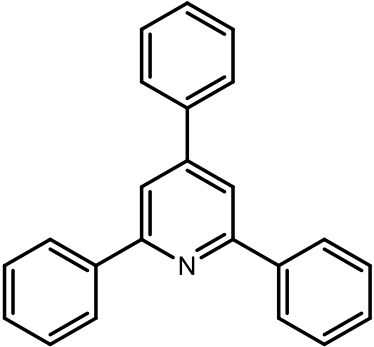
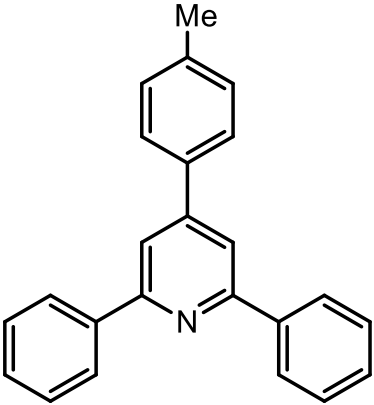
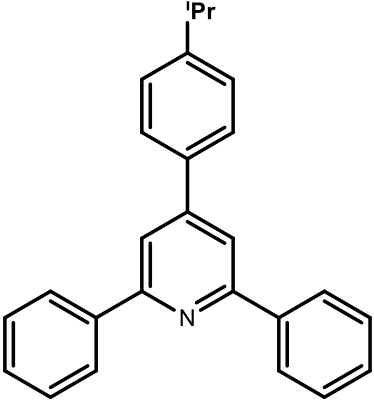
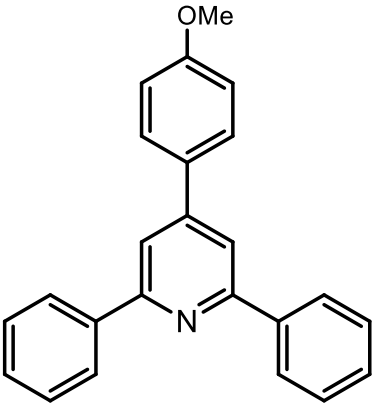
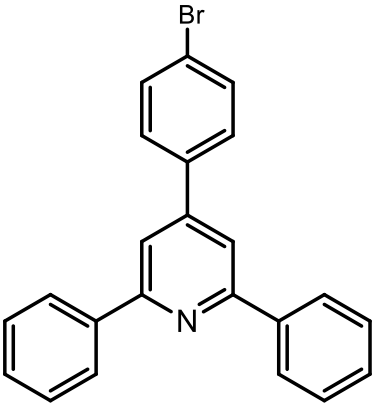
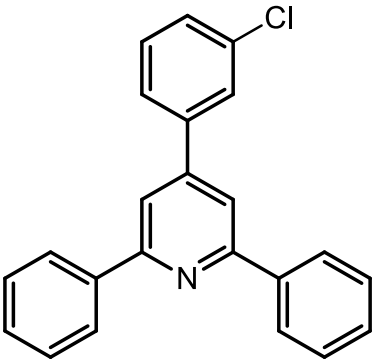
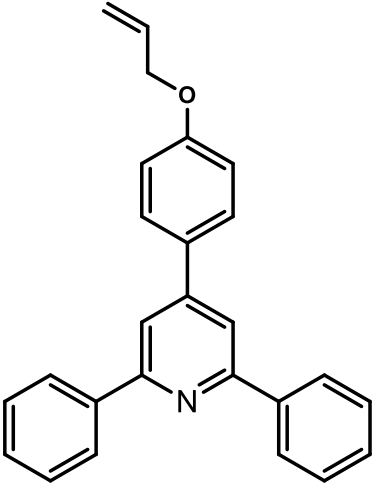
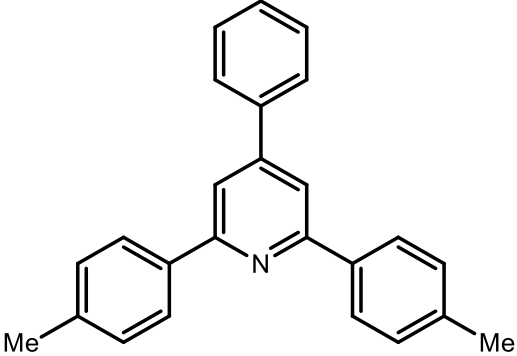
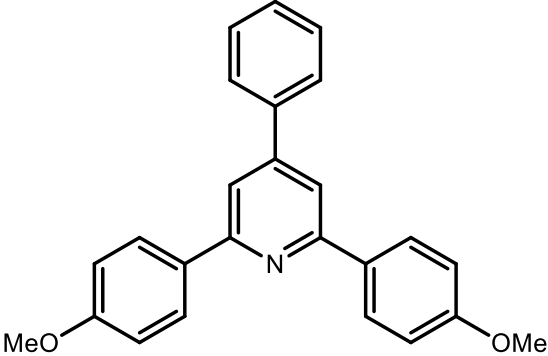


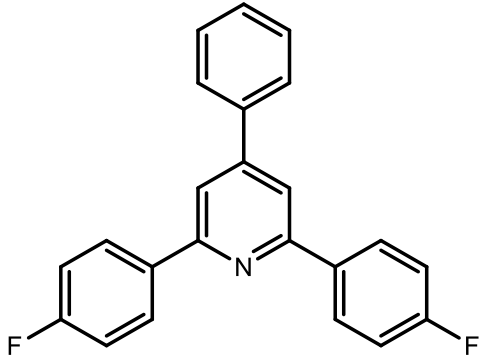
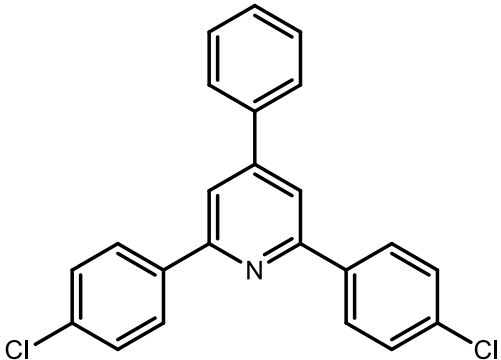
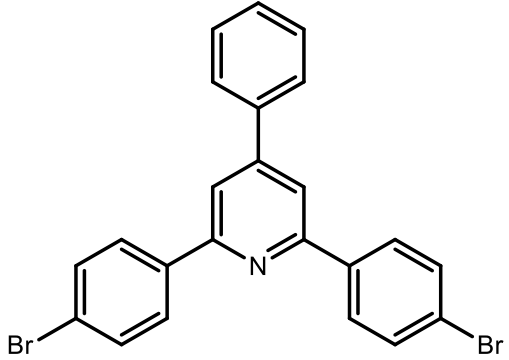
Figure S7. Recyclability test of the catalyst. The catalyst has been tested for further cycles. It was found that the activity of the catalyst was slowly decreasing may be due to the agglomeration of the nanoparticle after each cycle.

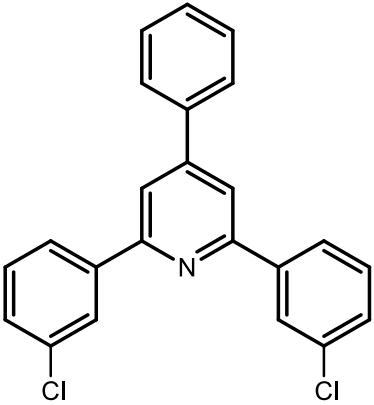
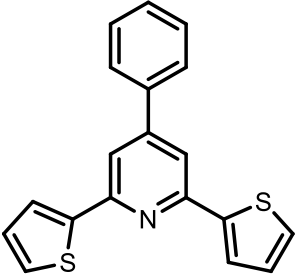
8. NMR data of the compounds

| | |
|---|---|
|  | <p>2,4,6-triphenylpyridine (Table 2, entry 1)¹ silica gel, hexane/ethyl acetate 99:1 White solid (80%) ¹H-NMR (500 MHz, CDCl₃) δ 8.20 (d, <i>J</i> = 7.6 Hz, 4H), 7.89 (s, 3), 7.75 (d, <i>J</i> = 6.9 Hz, 1H), 7.55-7.43 (m, 9H). ¹³C-NMR (125 MHz, CDCl₃) δ 157.6, 150.3, 139.7, 139.2, 129.2, 129.1, 128.8, 127.3, 127.2, 126.6, 117.2.</p> |
|  | <p>2,6-Diphenyl-4-(p-tolyl)pyridine (Table 2, entry 2)¹ silica gel, hexane/ethyl acetate 98:2 White solid (80%) ¹H-NMR (500 MHz, CDCl₃) δ 8.20 (d, <i>J</i> = 7.6 Hz, 4H), 7.89 (s, 2H), 7.66 (d, <i>J</i> = 8.0 Hz, 2H), 7.52 (t, <i>J</i> = 7.4 Hz, 4H), 7.45 (t, <i>J</i> = 7.4 Hz, 2H), 7.34 (d, <i>J</i> = 7.9 Hz, 2H), 2.45 (s, 3H) ¹³C-NMR (125 MHz, CDCl₃) δ 157.5, 150.2, 139.5, 139.2, 136.0, 129.9, 129.1, 128.7, 127.2, 127.0, 117.0, 21.3</p> |
|  | <p>4-(4-isopropylphenyl)-2,6-diphenylpyridine (Table 2, entry 3)¹ silica gel, hexane/ethyl acetate 98:2 White solid (75%) ¹H-NMR (500 MHz, CDCl₃) δ 8.24 (d, <i>J</i> = 7.2 Hz, 4H), 7.92 (s, 2H), 7.72 (d, <i>J</i> = 8.0 Hz, 2H), 7.55 (t, <i>J</i> = 7.4 Hz, 4H), 7.49–7.41 (m, 4H), 3.07–3.00 (m, 1H), 1.36 (d, <i>J</i> = 7.2 Hz, 6H) ¹³C-NMR (125 MHz, CDCl₃) δ 157.5, 150.2, 150.1, 139.7, 136.6, 129.0, 128.7, 128.6, 127.3, 127.2, 117.0, 34.0, 24.0</p> |

| | |
|---|--|
|  | <p>4-(4-methoxyphenyl)-2,6-diphenylpyridine (Table 2, entry 4)¹</p> <p>silica gel, hexane/ethyl acetate 98:2</p> <p>White solid (78%)</p> <p>¹H-NMR (500 MHz, CDCl₃) δ 8.20-8.18 (m, 4H), 7.85 (s, 2H), 7.71 (q, <i>J</i> = 3.1 Hz, 2H), 7.51 (t, <i>J</i> = 7.6 Hz, 4H), 7.44 (d, <i>J</i> = 6.9 Hz, 2H), 7.06-7.04 (m, 2H), 3.88 (s, 3H)</p> <p>¹³C-NMR (125 MHz, CDCl₃) δ 160.6, 157.6, 149.7, 139.8, 129.1, 128.9, 128.8, 128.4, 127.2, 116.7, 114.6, 55.5</p> |
|  | <p>4-(4-bromophenyl)-2,6-diphenylpyridine (Table 2, entry 5)¹</p> <p>silica gel, hexane/ethyl acetate 98:2</p> <p>White solid (74%)</p> <p>8.20 (d, <i>J</i> = 7.6 Hz, 4H), 7.84 (s, 2H), 7.64 (q, <i>J</i> = 9.3 Hz, 4H), 7.53 (t, <i>J</i> = 7.4 Hz, 4H), 7.46 (t, <i>J</i> = 6.8 Hz, 2H)</p> <p>¹³C-NMR (125 MHz, CDCl₃) δ 157.8, 150.3, 139.5, 139.1, 129.2, 129.1, 128.8, 128.7, 127.3, 127.2, 116.9</p> |
|  | <p>4-(3-chlorophenyl)-2,6-diphenylpyridine (Table 2, entry 6)³</p> <p>silica gel, hexane/ethyl acetate 98:2</p> <p>White solid (73%)</p> <p>¹H-NMR (500 MHz, CDCl₃) δ 8.21-8.19 (m, 4H), 7.87 (d, <i>J</i> = 22.1 Hz, 2H), 7.76-7.74 (m, 2H), 7.53-7.44 (m, 8H).</p> <p>¹³C-NMR (125 MHz, CDCl₃) δ 157.7, 148.8, 140.9, 139.3, 135.1, 130.4, 129.2, 128.9, 128.7, 127.3, 127.1, 125.3</p> |

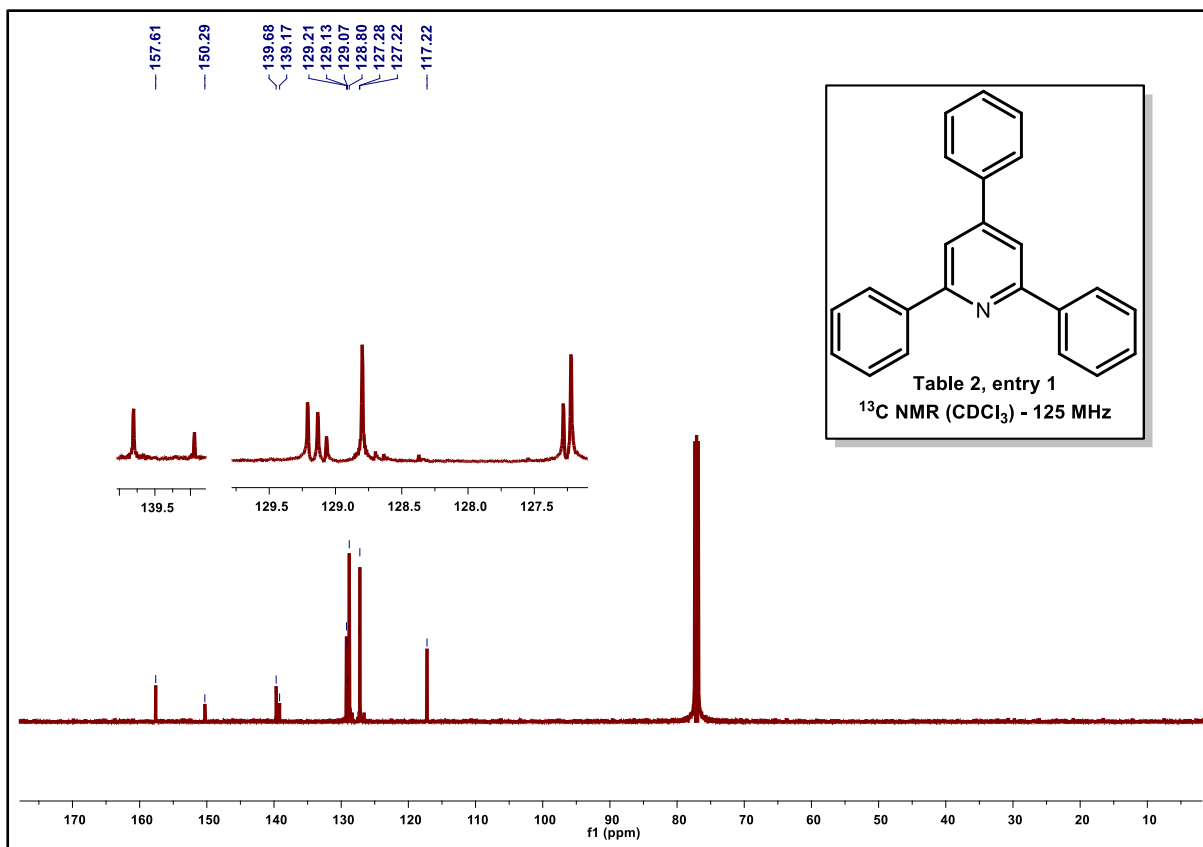
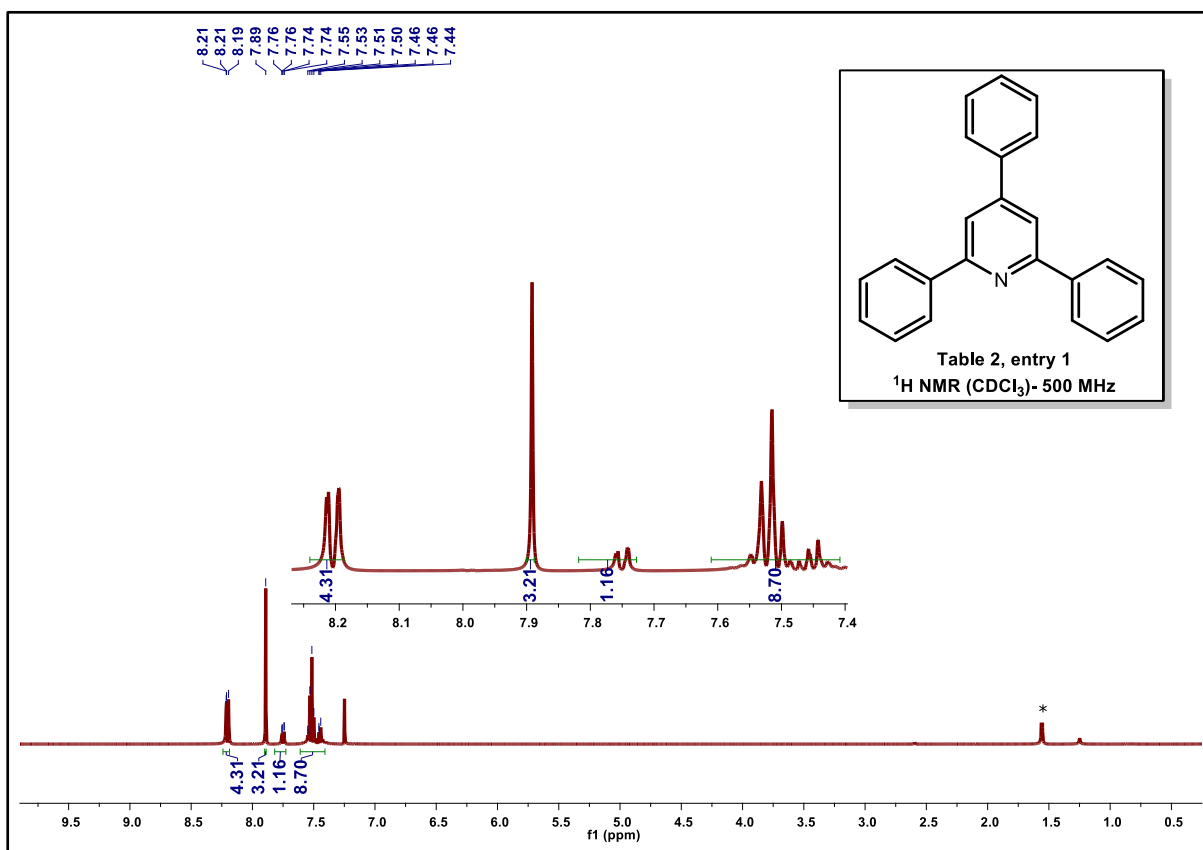
| | |
|---|---|
|  | <p>4-(4-(allyloxy)phenyl)-2,6-diphenylpyridine Table 2, entry 7)</p> <p>silica gel, hexane/ethyl acetate 98:2</p> <p>White solid (73%)</p> <p>¹H-NMR (500 MHz, CDCl₃) δ 8.20-8.16 (m, 4H), 7.85-7.82 (m, 2H), 7.70 (dd, <i>J</i> = 11.4, 3.1 Hz, 2H), 7.51 (t, <i>J</i> = 7.6 Hz, 4H), 7.45-7.42 (m, 2H), 7.07-7.04 (m, 2H), 6.09 (qd, <i>J</i> = 10.9, 5.3 Hz, 1H), 5.48-5.43 (m, 1H), 5.34-5.32 (m, 1H), 4.63-4.61 (m, 2H)</p> <p>¹³C-NMR (125 MHz, CDCl₃) δ 159.6, 157.6, 149.7, 139.8, 133.1, 131.5, 129.1, 128.8, 128.4, 127.2, 118.1, 116.7, 115.4, 69.0</p> |
|  | <p>4-phenyl-2,6-di-p-tolylpyridine (Table 3, entry 1)¹</p> <p>silica gel, hexane/ethyl acetate 99:1</p> <p>White solid (81%)</p> <p>¹H-NMR (500 MHz, CDCl₃) δ 8.09 (t, <i>J</i> = 3.8 Hz, 4H), 7.83 (s, 2H), 7.73 (dd, <i>J</i> = 6.9, 1.5 Hz, 2H), 7.52-7.46 (m, 3H), 7.31 (d, <i>J</i> = 8.4 Hz, 4H), 7.25 (s, 2H), 2.43 (d, <i>J</i> = 3.8 Hz, 6H)</p> <p>¹³C-NMR (125 MHz, CDCl₃) δ 157.5, 150.1, 139.0, 137.0, 129.5, 129.2, 128.9, 127.3, 127.1, 116.6, 21.4</p> |
|  | <p>2,6-bis(4-methoxyphenyl)-4-phenylpyridine (Table 3, entry 2)¹</p> <p>silica gel, hexane/ethyl acetate 98:2</p> <p>White solid (81%)</p> <p>¹H-NMR (500 MHz, CDCl₃) δ 8.10-8.08 (m, 4H), 7.70-7.66 (m, 4H), 7.47-7.39 (m, 3H), 6.96 (d, <i>J</i> = 8.4 Hz, 4H), 3.82 (s, 6H)</p> <p>¹³C-NMR (125 MHz, CDCl₃) δ 160.6, 157.1, 150.1, 139.5, 132.4, 129.1, 128.9, 128.5, 127.3, 115.8, 114.1, 55.5</p> |

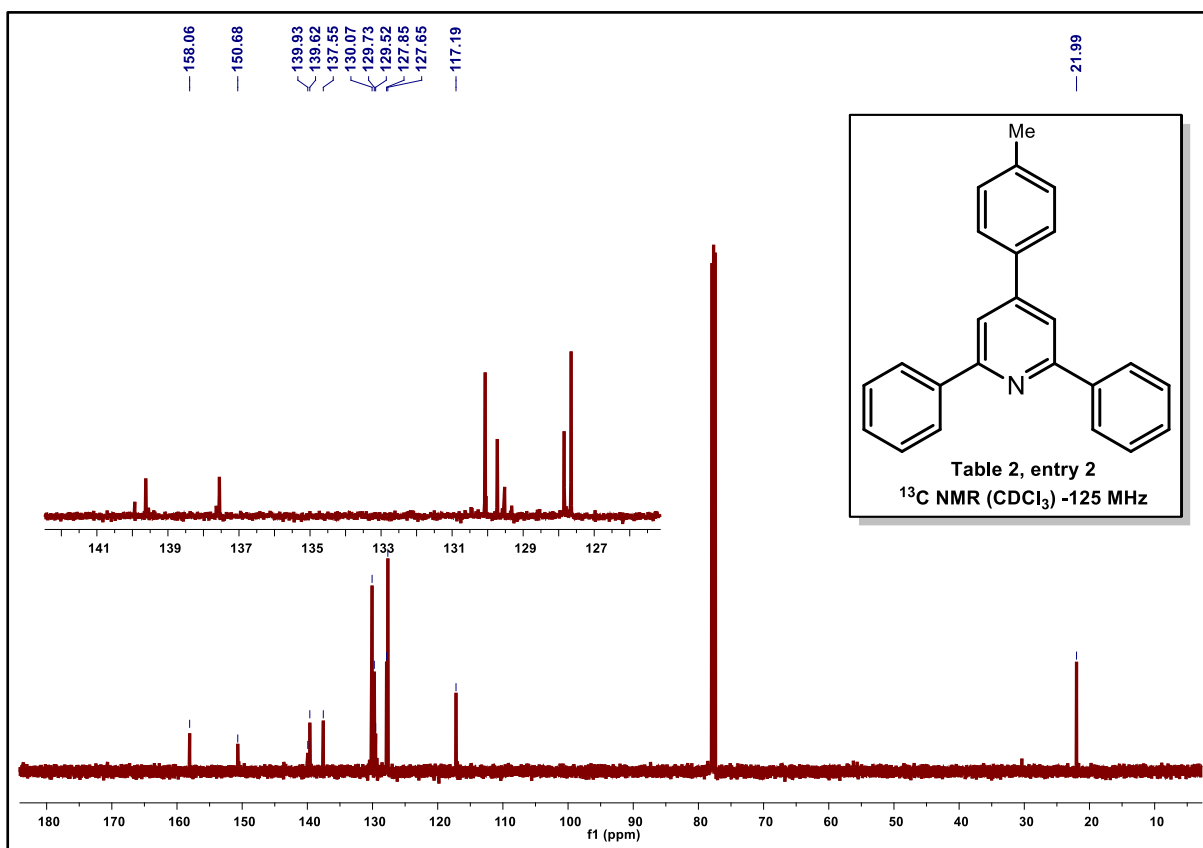
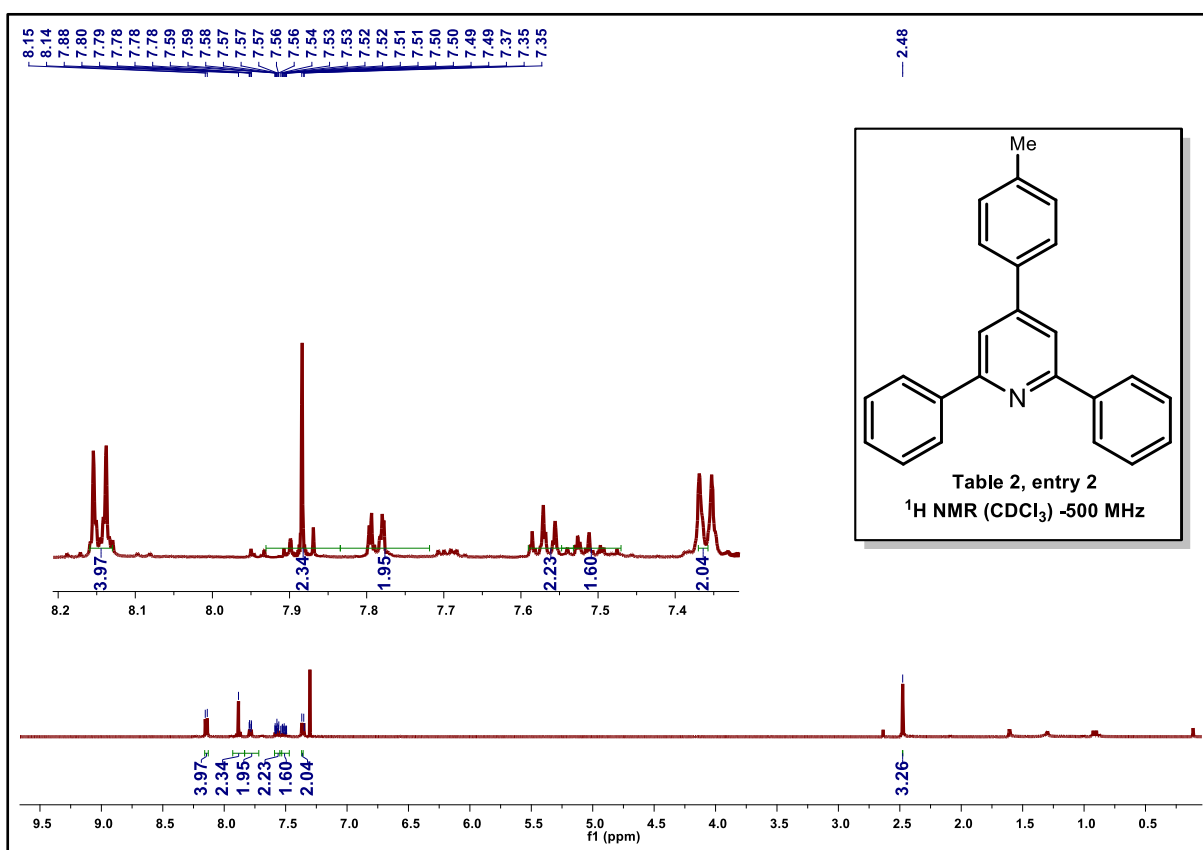
| | |
|---|---|
|  | <p>2,6-bis(4-fluorophenyl)-4-phenylpyridine (Table 3, entry 3)¹</p> <p>silica gel, hexane/ethyl acetate 98:2</p> <p>White solid (81%)</p> <p>¹H-NMR (500 MHz, CDCl₃) δ 8.17 (td, <i>J</i> = 6.1, 2.8 Hz, 4H), 7.82 (s, 2H), 7.77-7.72 (m, 2H), 7.54-7.48 (m, 3H), 7.21-7.17 (m, 4H)</p> <p>¹³C-NMR (125 MHz, CDCl₃) δ 164.7, 162.7, 156.6, 150.6, 138.9, 135.7, 131.0, 129.2, 129.2, 129.0, 128.9, 127.2, 116.8, 115.8, 115.6, 77.3, 77.1, 76.8, 29.8</p> |
|  | <p>2,6-bis(4-chlorophenyl)-4-phenylpyridine Table 3, entry 4)¹</p> <p>silica gel, hexane/ethyl acetate 98:2</p> <p>White solid (81%)</p> <p>¹H-NMR (500 MHz, CDCl₃) δ 8.13-8.10 (m, 4H), 7.83 (d, <i>J</i> = 24.4 Hz, 2H), 7.66 (d, <i>J</i> = 8.4 Hz, 1H), 7.51-7.47 (m, 6H)</p> <p>¹³C-NMR (125 MHz, CDCl₃) δ 156.3, 150.8, 138.6, 137.5, 135.4, 129.3, 129.2, 128.9, 128.5, 127.1, 117.3</p> |
|  | <p>2,6-bis(4-bromophenyl)-4-phenylpyridine (Table 3, entry 5)¹</p> <p>silica gel, hexane/ethyl acetate 98:2</p> <p>White solid (81%)</p> <p>¹H-NMR (500 MHz, CDCl₃) δ 8.07-8.03 (m, 4H), 7.86 (s, 1H), 7.81 (s, 1H), 7.73-7.71 (m, 1H), 7.67-7.58 (m, 5H), 7.55-7.48 (m, 2H)</p> <p>¹³C-NMR (125 MHz, CDCl₃) δ 157.5, 150.1, 139.4, 139.2, 129.2, 129.1, 128.7, 127.3, 127.0, 126.6, 117.0.</p> |

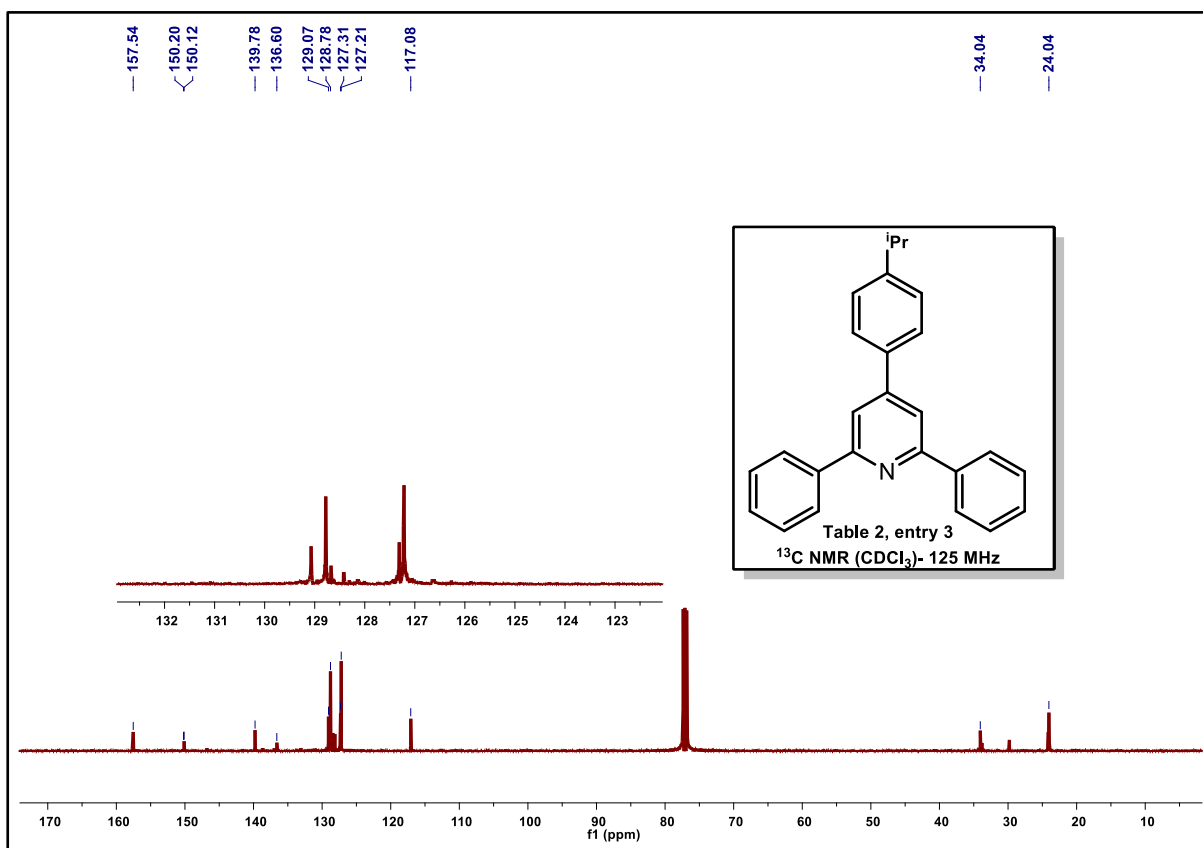
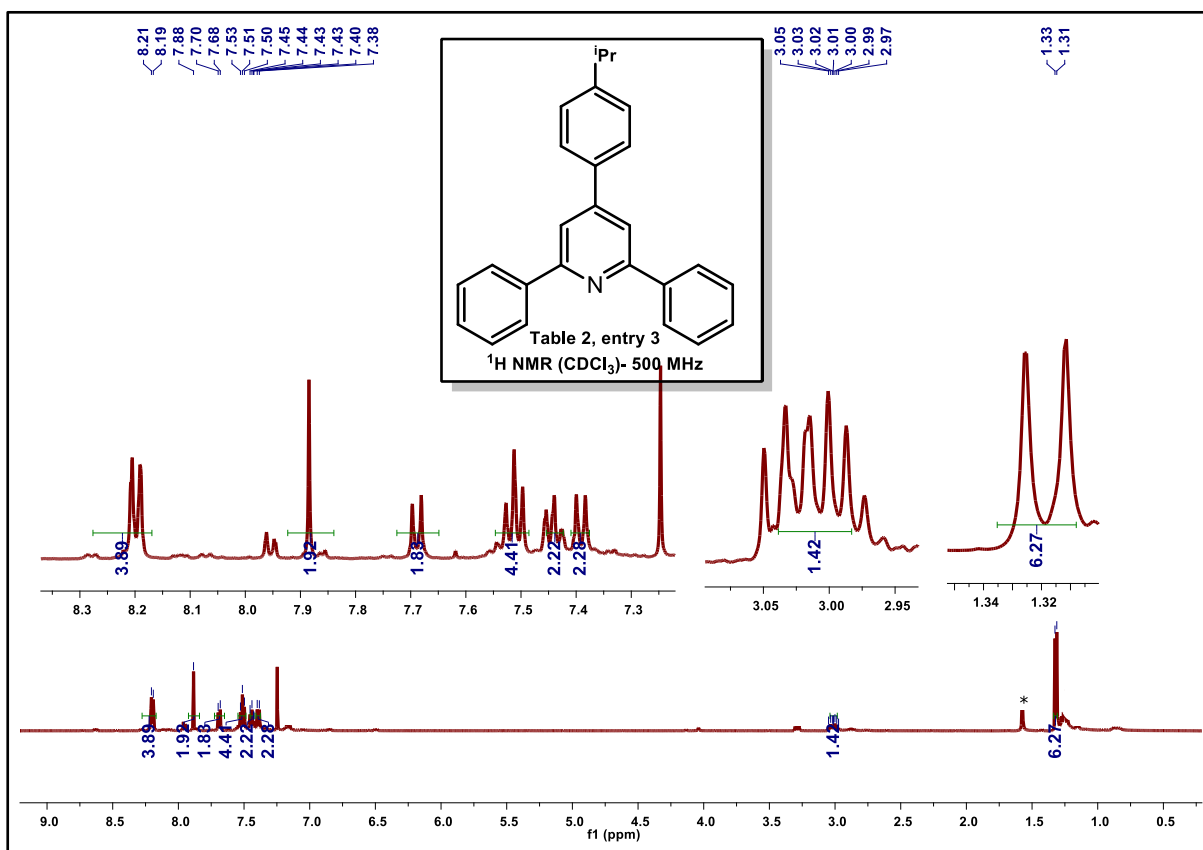
| | |
|--|--|
|  | <p>2,6-bis(3-chlorophenyl)-4-phenylpyridine (Table 3, entry 6)¹</p> <p>silica gel, hexane/ethyl acetate 98:2</p> <p>White solid (71%)</p> <p>¹H-NMR (500 MHz, CDCl₃) δ 8.18 (s, 2H), 8.06 (d, <i>J</i> = 6.8 Hz, 2H), 7.88 (s, 2H), 7.74 (d, <i>J</i> = 6.8 Hz, 2H), 7.56–7.44 (m, 7H)</p> <p>¹³C-NMR (125 MHz, CDCl₃) δ 156.2, 150.7, 141.1, 138.5, 134.9, 130.2, 129.3, 129.2, 129.2, 127.3, 127.2, 125.2, 117.7</p> |
|  | <p>4-phenyl-2,6-di(thiophen-2-yl)pyridine (Table 3, entry 6)¹</p> <p>silica gel, hexane/ethyl acetate 98:2</p> <p>White solid (81%)</p> <p>¹H-NMR (500 MHz, CDCl₃) δ 7.71–7.66 (m, 4H), 7.54–7.47 (m, 2H), 7.42 (t, <i>J</i> = 2.7 Hz, 2H), 7.25 (s, 2H), 7.13 (q, <i>J</i> = 3.1 Hz, 2H)</p> <p>¹³C-NMR (125 MHz, CDCl₃) δ 152.6, 150.2, 144.9, 138.6, 129.1, 127.9, 127.2, 127.1, 124.9, 115.1</p> |

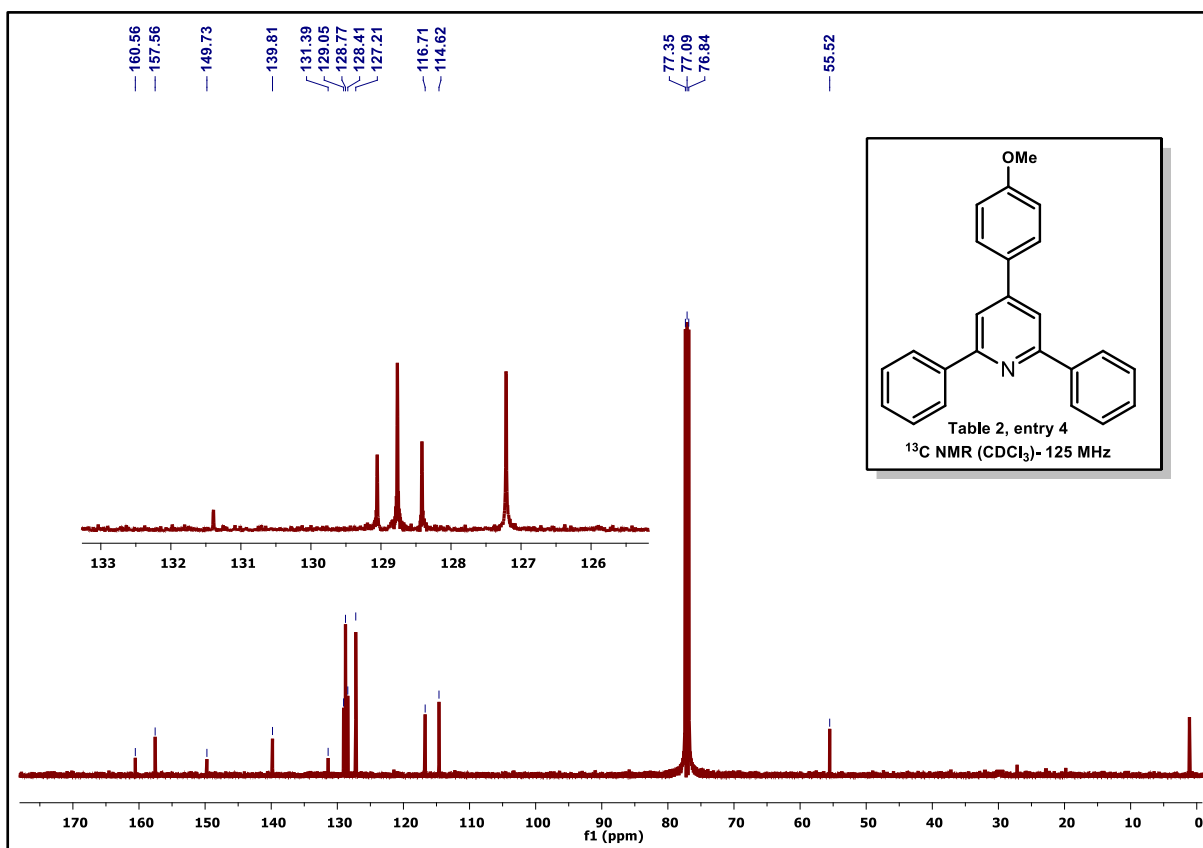
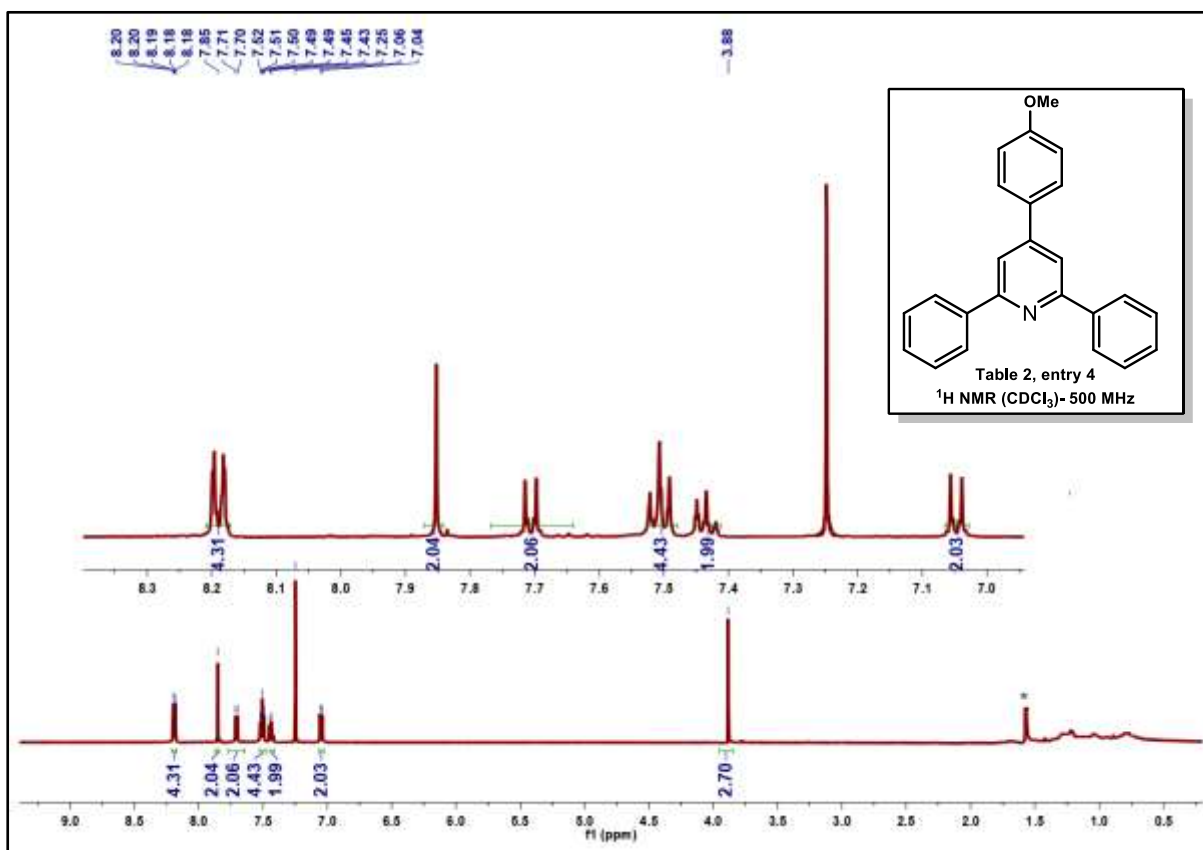
9. Reference

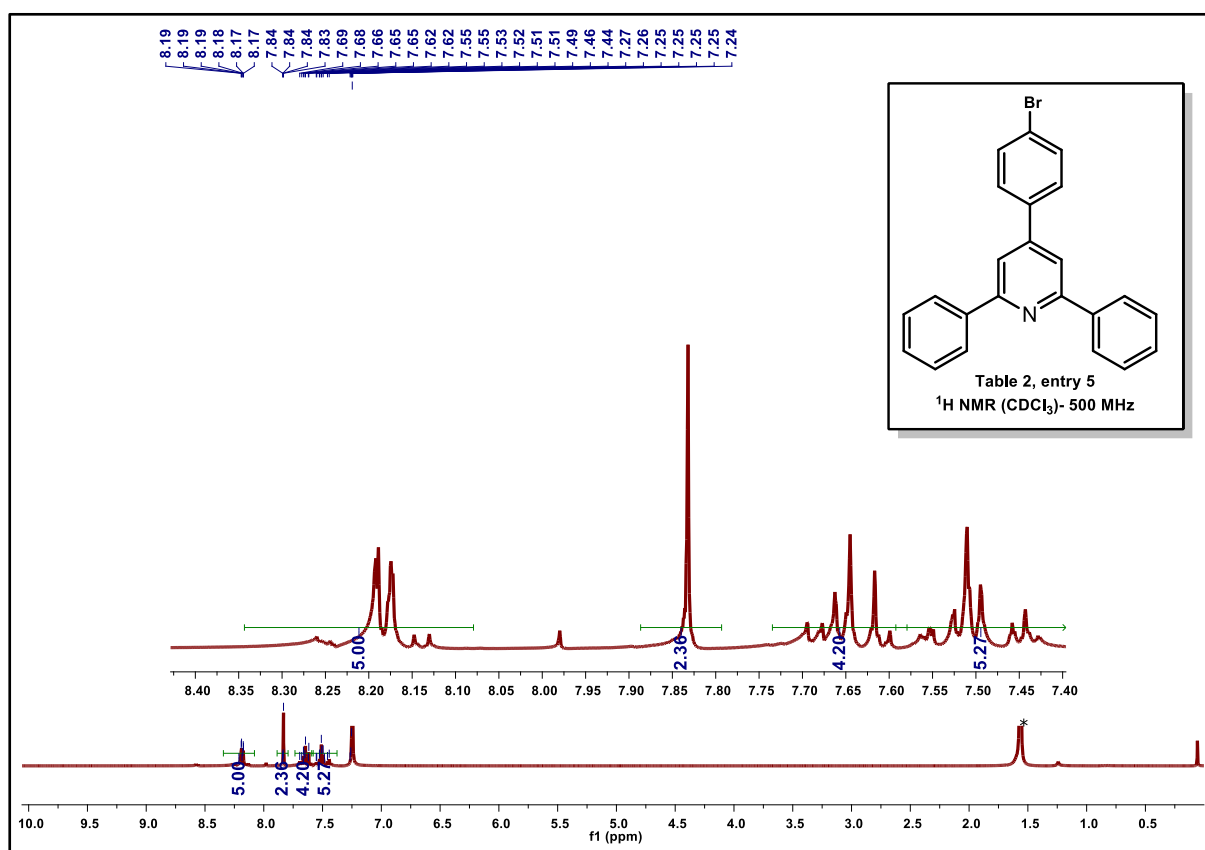
1. S. Pal, S. Das, S. Chakraborty, S. Khanra, and N.D. Paul, *J. Org. Chem.* 2023, **88**, 3650-3665.
2. R.S. Rohokale, B. Koenig, and D.D. Dhavale, *J. Org. Chem.* 2016, **81**, 7121-7126.
3. J. Han, X. Guo, Y. Liu, Y. Fu, R. Yan, and B. Chen, *Adv. Synth. Catal.* 2017, **359**, 2676-2681.

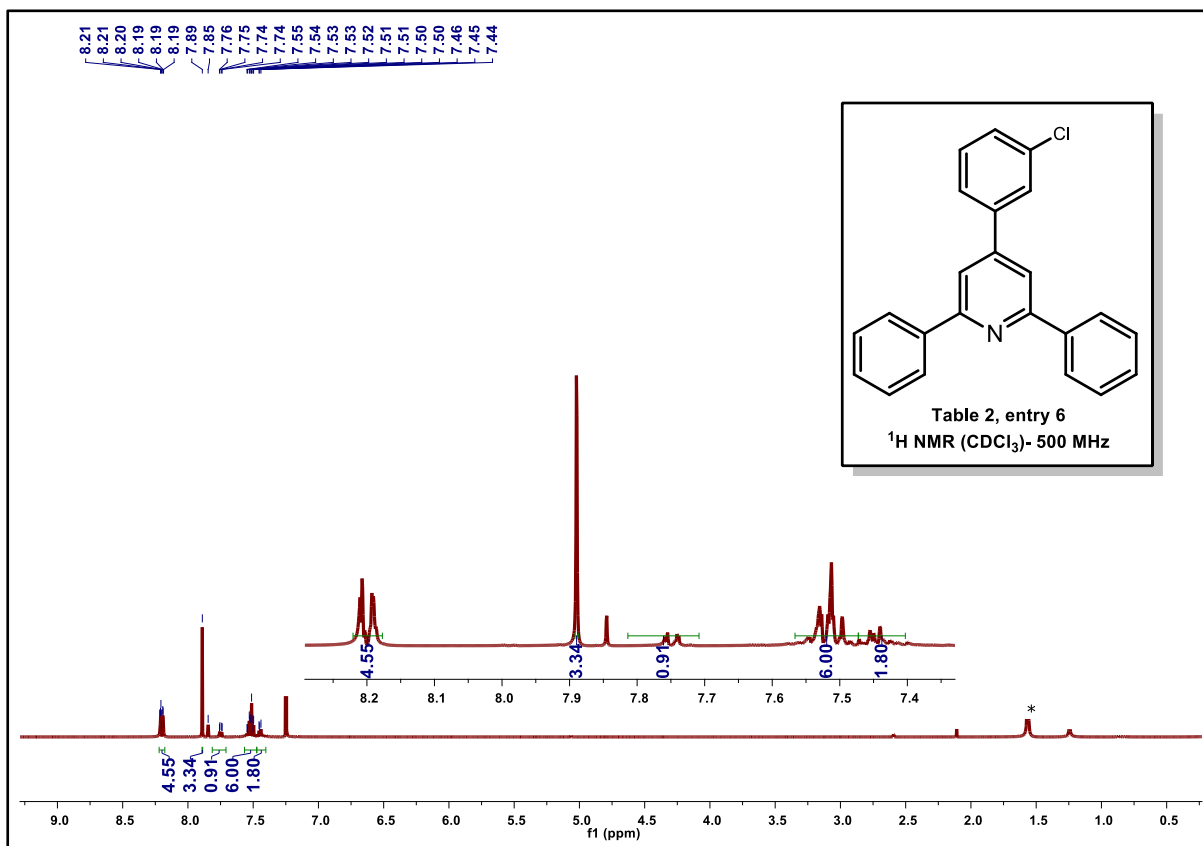
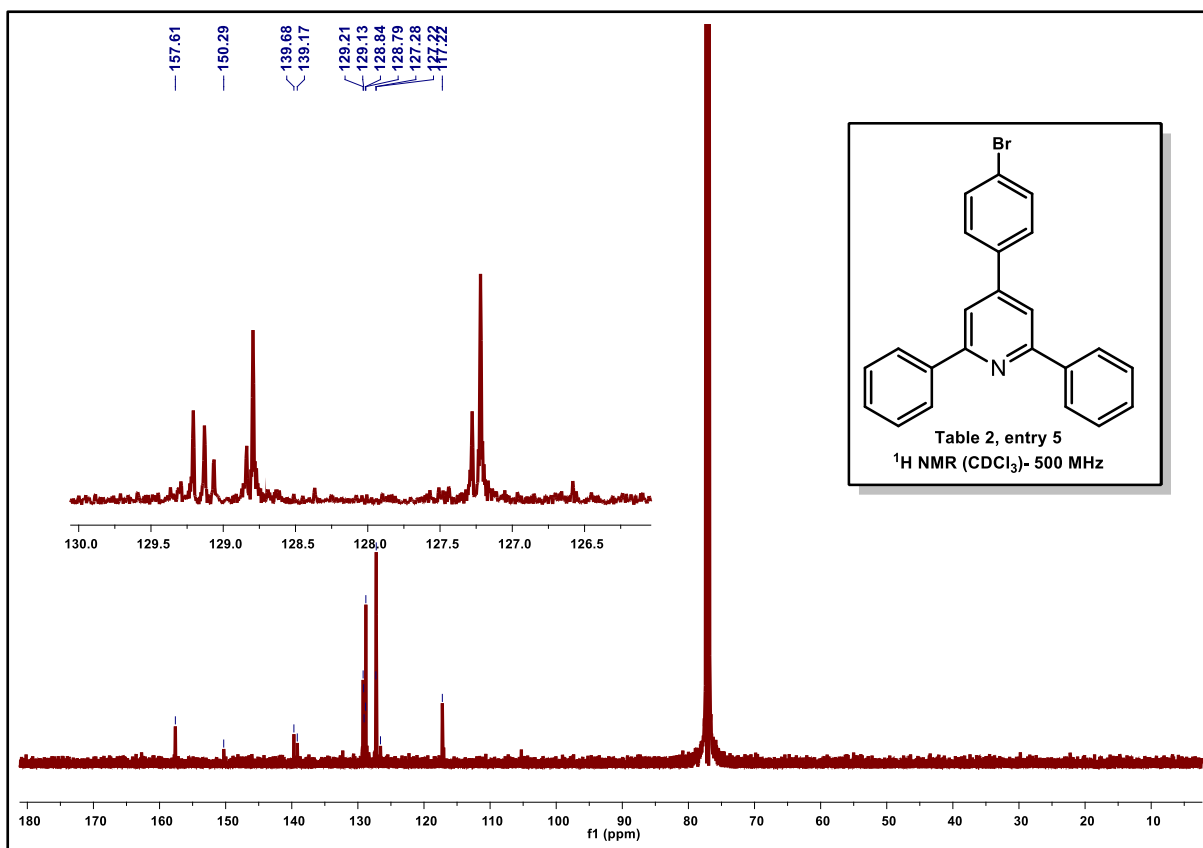


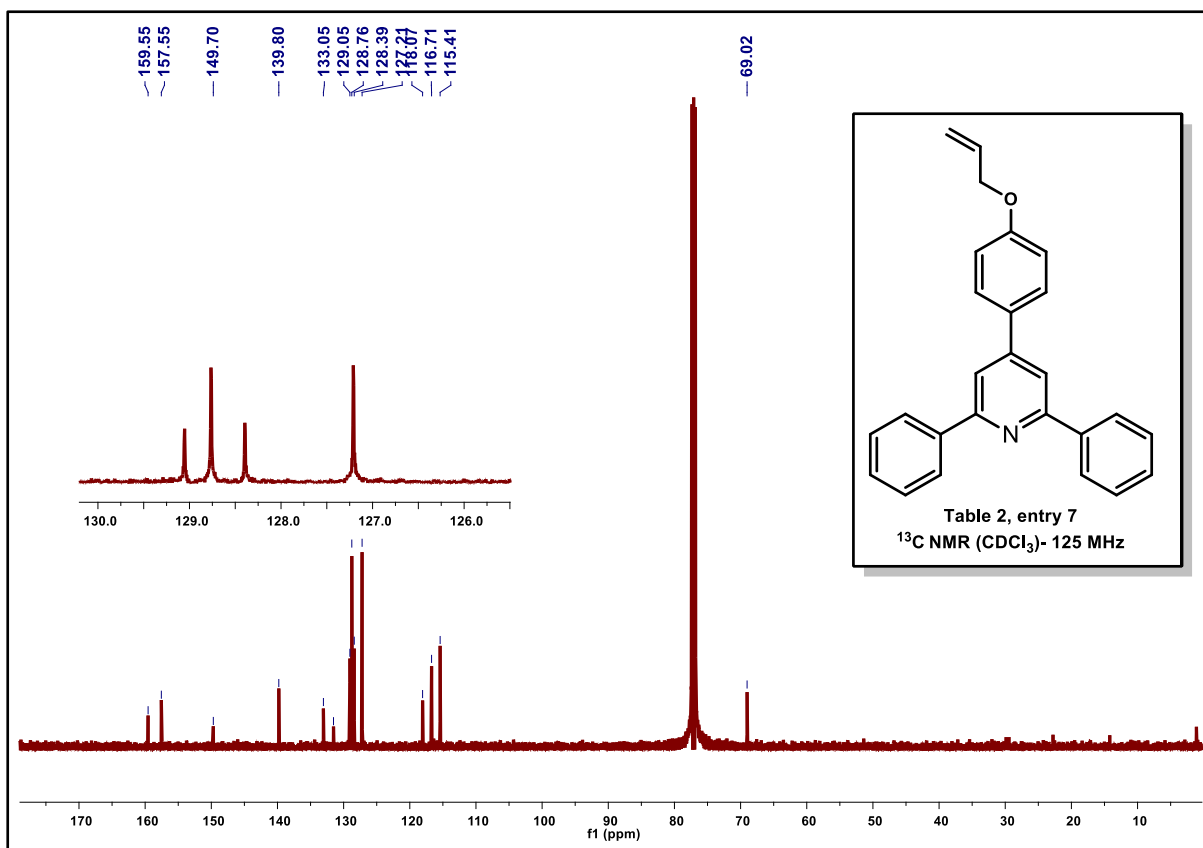












(* Moistur

